JOURNAL OF AIRCRAFT
Vol. 31, No. 1, Jan.–Feb. 1994

Computational Study of Transition Front on a Swept Wing Leading-Edge Model

Venkit Iyer*
ViGYAN, Inc., Hampton, Virginia 23666
Robert E. Spall†
University of South Alabama, Mobile, Alabama 36688
and
J. Ray Dagenhart‡
NASA Langley Research Center, Hampton, Virginia 23665

The linear stability of fully three-dimensional supersonic boundary layers formed over a swept wing leading-edge region was investigated. The geometry represents a model which is to be utilized for transition studies in the NASA Langley $M = 3.5$ supersonic low-disturbance pilot tunnel. Estimates of the location of the onset of transition were made using the e^N method with mean flow profiles computed as solutions to the Navier-Stokes equations. Modes with the highest integrated amplification rates were traveling crossflow disturbances with frequencies in the range of 30–40 kHz. Calculations were performed with parametric changes in angle of attack, freestream Reynolds number, boundary-layer suction levels, and wall cooling. The influence of these parameters on transition is important in the design optimization of natural or forced laminar flow control on a swept supersonic wing. Distributed suction was found to stabilize the boundary layer to below $N = 10$ levels over the entire model. Wall cooling and reduced freestream Reynolds numbers also had stabilizing effects. Increase in angle of attack had only a mildly destabilizing effect for this model in the range studied.

Nomenclature

C_p = pressure coefficient
M_∞, U_∞ = freestream Mach number and velocity
N = N factor
P = pressure
q_s = suction rate, $(\rho_w v_w)/(\rho_\infty U_\infty)$
Re_{CF} = crossflow Reynolds number, $(v^*_{CF,max})(\delta^*_{0.1})/(\nu^*_e)$
Re_∞ = freestream Reynolds number per unit length, U_∞/ν_∞
s = arc length along surface from neutral point to transition
T = temperature
u, v, w = velocities in the streamwise, spanwise, and normal directions
$\bar{V}_g$ = complex group velocity
v_{CF} = velocity in the crossflow direction (orthogonal to the local edge streamline)
X, Y, Z = Cartesian coordinates
x, y, z = boundary-layer coordinates in streamwise, spanwise, and normal directions
α = angle of attack
$\bar{\alpha}$, $\bar{\beta}$ = wave numbers
$\delta^*_{0.1}$ = value of z^* above which $v_{CF} < 0.1\ v_{CF,max}$
$\delta^*_{0.995}$ = boundary-layer thickness corresponding to 99.5% of edge absolute velocity
λ = wavelength
ν = kinematic viscosity
ρ = density
σ = spatial growth rate
ψ = wave orientation
ω_i = temporal growth rate
ω_r = real frequency

Subscripts
c = neutral point
e = boundary-layer edge
t = transition point
w = wall quantity
$'$ = $\partial/\partial z$
∞ = freestream quantity

Superscripts
$*$ = dimensional quantity
$\hat{}$ = sinusoidal component

Introduction

LAMINAR flow control (LFC) by passive, active, or hybrid techniques has the potential for achieving significant fuel savings in future supersonic transports.[1] However, the technical challenges in achieving significant amounts of laminar flow on a highly swept supersonic wing are substantial. In addition to streamwise amplification of disturbances of the Tollmien-Schlichting (TS) type, the high degree of sweep generates a substantial amount of crossflow within the boundary layer (BL). This leads to the amplification of crossflow disturbances as another route to transition to turbulence.

The design of a supersonic swept wing with large extent of laminar flow is a function of many parameters such as sweep angle, angle of attack, freestream Reynolds number, and wing cross section. Attachment line contamination and the resulting leading-edge transition are also important factors in swept wing design. In addition, incorporation of active LFC involves parameters such as suction rate and its distribution, as well as the wall temperature. Real world application is further influenced by wing surface quality (waviness and roughness) and receptivity to freestream turbulence and acoustic disturbances.

Received May 7, 1992; presented as Paper 92-2630 at the AIAA 10th Applied Aerodynamics Conference, Palo Alto, CA, June 22–24, 1992; revision received Sept. 10, 1992; accepted for publication Oct. 26, 1992.

*Senior Research Scientist, 30 Research Drive. Member AIAA.
†Assistant Professor, Department of Mechanical Engineering. Member AIAA
‡Aerospace Engineer, Experimental Flow Physics Branch, Fluid Mechanics Division, M/S 163. Member AIAA.

A key factor in the design of LFC applications is the ability to accurately estimate the location of the onset of transition over complicated geometries. This is a difficult task and is a subject of current research in high-speed aerodynamics. Methods commonly used in the aircraft industry for transition prediction are often based on simple correlations such as maximum values for the momentum thickness and crossflow Reynolds numbers. If more reliable estimates are needed, as in the present work, linear stability theory and the e^N method may be employed.[2] The method relies on correlations between the most amplified single normal mode disturbances and experimentally determined locations for the onset of transition. Linear stability calculations can provide useful information regarding the effect of angle of attack, Reynolds number, wall cooling/heating, suction/blowing, etc. on boundary-layer stability. However, the method cannot account for such important factors as receptivity to freestream disturbances and surface roughness.

Most previous studies employing linear stability theory have been restricted to two-dimensional or axisymmetric flows, or have considered simple three-dimensional mean flows (e.g., rotating disk, swept wing with straight isobars etc.). A concise summary of many of these studies has been given by Malik.[3] The limitations have been primarily due to the difficulty in obtaining the accurate mean flows necessary for meaningful stability analysis over complicated geometries. Exceptions to these limitations include the linear stability calculations of fully three-dimensional low-speed boundary layers over fuselage-type configurations.[4-6] The development of accurate solution algorithms for high-speed flows based on the solution of the Navier-Stokes (NS) equations means that stability analysis of a wider variety of practical configurations is now possible. Thus, taken together, accurate NS solution algorithms and linear stability theory can provide important design tools for future LFC applications.

For the work to be presented here, linear stability theory and the e^N method were used to estimate the location of the onset of transition for an experimental model of a supersonic swept wing leading edge. The mean flow of highly swept wings is strongly three-dimensional. Since the infinite swept wing approximation was not strictly valid in this case, the approach used here is to compute the mean flow by solving the NS equations. The resulting profiles were then recast in boundary-layer coordinates and stability calculations were performed using a version of the linear stability code COSAL (modified to accept fully three-dimensional boundary layers).[7] Analysis of linear stability with parametric changes in freestream conditions (α, Re_∞) was carried out. The effectiveness of stabilizing streamwise and crossflow instabilities by wall suction and cooling (parametric changes in q_s and T_w) was also investigated. The effect of normal grid refinement on stability prediction was also determined.

Experimental transition studies on the model are being performed in the NASA Langley $M = 3.5$ supersonic low-disturbance pilot tunnel (SSLDPT). Results of the present study are being used to determine the test envelope, instrumentation, and measurement requirements for the experimental study.

Numerical Method

The goal of linear stability theory is to determine the response of a predetermined mean flow to an infinitesimally small disturbance. In this work, the mean flow is taken to be the solution of the compressible thin-layer NS equations. Due to the presence of large crossflow, crossflow reversal, and difficulty of specifying accurate initial and side boundary profiles, three-dimensional boundary-layer solutions do not provide the accuracy required in the present case. A finite volume upwind-differenced NS solver (CFL3D) has been employed for this purpose.[8] The code has been extensively used for flow calculations at Mach numbers ranging from subsonic to hypersonic. Reference 9 discusses the accuracy of the code when compared with a central-differenced solver. Mean flow solutions are calculated in terms of Cartesian velocities, temperature, and density profiles based on a general curvilinear grid. To perform the stability analysis, boundary-layer-type contravariant velocity profiles on a surface-normal grid are needed. This transformation is accomplished through an interface program. Details of this interface program and an assessment of the accuracy of the solutions generated using CFL3D for the purpose of stability calculations are given in Ref. 10.

The linear stability analysis of three-dimensional compressible boundary layers involves the solution of an eigenvalue problem for an eighth-order system of ordinary differential equations. These equations are derived from the compressible NS equations using small disturbance theory. Flow variables are each decomposed into a steady term and an infinitesimally small term of sinusoidal form, and are substituted into the NS equations. By assuming a locally parallel flow, and by neglecting higher order terms and subtracting out the terms for the undisturbed steady mean flow, a set of five ordinary differential equations is obtained. The set may be expressed as

$$\left(A\frac{d^2}{dz^2} + B\frac{d}{dz} + C\right)\bar{\phi} = 0 \tag{1}$$

where $\bar{\phi}$ is a five-element vector defined by $[\tilde{\alpha}\hat{u} + \tilde{\beta}\hat{v}, \hat{w}, \hat{P}, \hat{T}, \tilde{\alpha}\hat{v} - \tilde{\beta}\hat{u}]$. The elements of the A, B, C matrices are given in Malik and Orzag.[11] From the set of five equations (Eq. 1), it is possible to obtain (by eliminating pressure) a set of four second-order equations or a system of eight first-order ordinary differential equations (although in the present analysis, the equations are solved in their original form). The system is solved subject to the boundary conditions:

$$\begin{aligned} &\phi_1 = \phi_2 = \phi_4 = \phi_5 = 0 \quad \text{at} \quad z = 0 \\ &\phi_1, \phi_2, \phi_4, \phi_5 \to 0 \quad \text{as} \quad z \to \infty \end{aligned} \tag{2}$$

In the present work, the equations are solved using a modified version of the computer code COSAL which utilizes a second-order finite difference formulation on a staggered grid, eliminating the need for pressure boundary conditions.

Given the Reynolds number, the above system provides a complex dispersion relation of the form

$$\omega = \omega(\tilde{\alpha}, \tilde{\beta}) \tag{3}$$

For the temporal formulation used in COSAL, wave numbers $\tilde{\alpha}$ and $\tilde{\beta}$ are real, while ω is complex. The dispersion relation contains four arbitrary parameters: $\tilde{\alpha}$, $\tilde{\beta}$, ω_i, and ω_r. Two conditions are provided by the complex dispersion relation. Two more conditions are needed to remove the arbitrariness in the problem. One is that the real frequency f is held constant, which fixes ω_r. The second results from the requirement that ω_i be maximized with respect to the wave orientation and the wavelength (the "envelope method").

To compute the N factors, the temporal growth rate is transformed to a spatial growth rate using the group velocity transformation[12]

$$\sigma = [\omega_i/|Re(\bar{V}_g)|] \tag{4}$$

The N factors used in transition correlation are then computed as

$$N = \int_{s_c}^{s_t} \sigma \, ds \tag{5}$$

The integration is carried out in the direction of the group velocity vector.

Table 1 Summary of cases studied

Case 1	Baseline case: α = 0 deg, Re_∞ = 2.4 million/ft, q_s = 0, $T_w = T_{adiabatic}$
Case 2, 3, or 4	Same as case 1, except α = 1.5, 3, or 4.5 deg
Case 5	Case 1 with uniform suction, q_s = 0.0004
Case 6	Case 1 with distributed suction, q_s = 0.0012 ↓ 0.0001
Case 7 or 8	Same as case 1, except T_w/T_∞ = 2 or 2.6 (cold wall)
Case 9, 10, or 11	Same as case 1, except Re_∞ = 1.2, 4, or 6 million/ft
Case 12	Case 1 with larger normal grid resolution

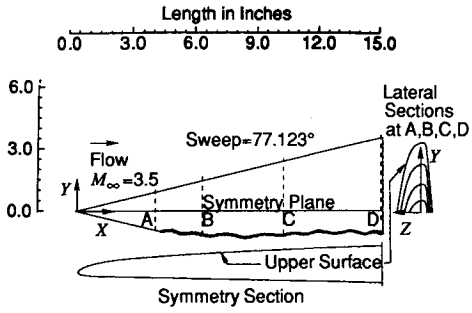

Fig. 1 Supersonic swept leading-edge geometry.

Geometry and Conditions

The geometry corresponds to a 15-in. model of a supersonic swept wing leading edge which is installed in the NASA Langley SSLDP Tunnel. The leading-edge sweep is 77.1 deg, resulting in a leading-edge normal Mach number of 0.78. The model (Fig. 1) is a laterally symmetric representation of the first 6.25% chord region of a highly swept supersonic wing.

The nominal conditions at which calculations were initially obtained are as follows: α = 0 deg, P_∞ = 39.3 psf, T_∞ = 162.3°R. This results in a Re_∞ value of 2.4 million/ft. The wall condition for this "baseline" case is adiabatic and zero suction. Several other cases corresponding to one-parameter changes relative to the baseline case were considered. The purpose of these additional calculations was to investigate the effect of control techniques such as wall suction and wall cooling on the stability of the boundary layer. Effects of varying the angle of attack and Re_∞ were also investigated. Grid resolution studies were also performed. A summary of these cases is given in Table 1. The Navier-Stokes code employed (CFL3D) is a vectorized code optimized for CRAY application. In all the cases considered (including suction cases), full convergence was obtained in 2–3 h of CPU time. Convergence was accelerated by use of the multigrid option in the code, time-stepping and by the use of the maximum allowable CFL numbers. Convergence was assured by monitoring the profiles, skin friction, and wall temperature values until they showed little change with iteration. Convergence is also accelerated by using a converged result from another appropriate case as the starting solution.

Results

In all cases, the grid employed for the calculation of the mean flow contained 97 points in the spanwise direction and 53 points in the streamwise direction. The number of points included within the boundary layer in the wall-normal direction varied with respect to the location on the wing leading edge, but was generally about 30. An assessment of the grid resolution in the wall-normal direction is given at the end of this section. The results presented here are for the upper surface on the wing, since this is the region of principal importance in LFC applications.

Figure 2a shows a contour plot of the pressure coefficient distribution on the upper surface for the baseline case (note

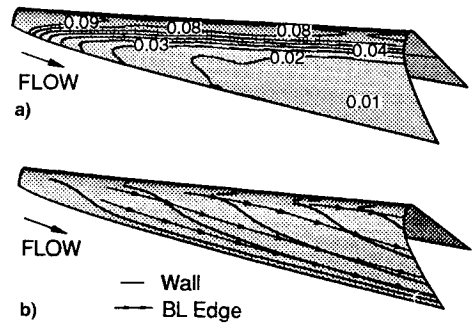

Fig. 2 Swept leading-edge case 1 mean flow results: a) pressure coefficient on upper surface and b) boundary-layer edge and limiting (wall) streamlines.

that the upper surface is shown upside down in this and the following figures to better show the region of interest). The pressure contours are essentially parallel to the leading edge, except very near the apex and the symmetry plane. This large pressure gradient normal to the attachment line, coupled with the high degree of wing sweep, gives rise to large levels of crossflow within the boundary layer. In Fig. 2b limiting streamlines at the wall and the boundary-layer edge streamlines are shown. The large extent of turning of the flow in the boundary layer near the attachment line is evident. At its maximum, the crossflow velocity is approximately 8% of the edge velocity. This turning, or crossflow, develops due to the deflection of the low-momentum fluid near the wall in the direction of decreasing pressure.

The crossflow Reynolds number is often used as a parameter to correlate transition. For incompressible flows, a Re_{CF} value of 200 represents an approximate upper limit for the existence of laminar flow.[7,13] As compressibility becomes important, this upper limit on crossflow Reynolds number increases drastically.[14] This is due primarily to the effect of Mach number on boundary-layer thickness, and hence, the length scale used in the definition of Re_{CF}. Taking this into account, a scaled crossflow Reynolds number may be defined as, $Re_{CF} = [1 + M_e^2(\gamma - 1)/2]Re_{CF,i}$, where $Re_{CF,i}$ is the incompressible value with an upper limit of 200 for laminar flow. For the present case ($M_e \approx 3.2$), this results in an upper limit of 500–600 for Re_{CF}.

Plotted in Fig. 3a are contours of constant crossflow Reynolds number for the baseline case. Maximum values are in the range of 500, and therefore, it is expected that crossflow will have a large influence on the stability of the boundary layer. Shown in Fig. 3b are contours of Re_{CF} for α = 4.5 deg (case 4). Here, it is noted that the maximum values of Re_{CF} have increased to 1200 and that the levels near the leading edge are also much higher. The increase in Re_{CF} near the symmetry plane indicates crossflow reversal resulting from the suction peak which begins to develop at this higher angle of attack. The effect of this on the stability and (estimated) transition front of the boundary layer is of interest. Shown in Fig. 4a is the spanwise variation of C_p at X = 14.8-in. from the apex for cases 1–4 as α is increased. Figure 4b is a corresponding plot of the displacement thickness. The larger pressure gradients with increasing α create larger crossflow while the boundary layer also thickens appreciably, both factors being destabilizing. The α = 3 and 4.5-deg cases also show suction peaks, causing the crossflow to reverse near these locations, as noted previously.

Presented in Figs. 5a and 5b are a series of N factor traces for the configuration designated as case 1. Each trace represents a series of eigenvalue calculations at approximately 20 streamwise locations. The mode computed at each location was such that the growth rate was maximized with respect to wave angle and wavelength (the envelope method). The integration path to the next location was given by the direction

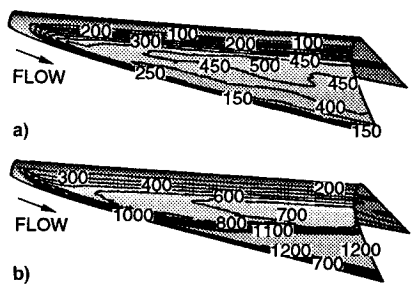

Fig. 3 Crossflow Reynolds number on the upper surface of swept leading edge, M_∞ = 3.5, Re_∞ = 2.4 million/ft: a) α = 0 deg and b) α = 4.5 deg.

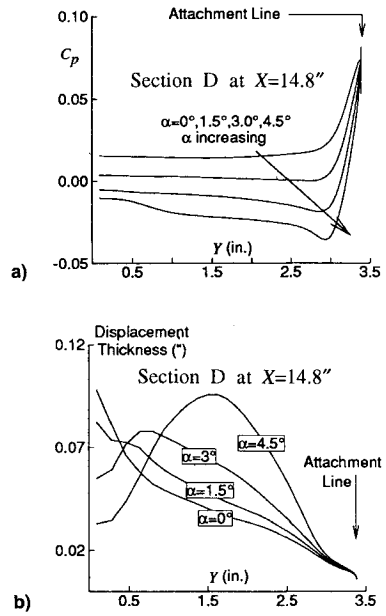

Fig. 4 Spanwise variation of a) C_p and b) displacement thickness, with α.

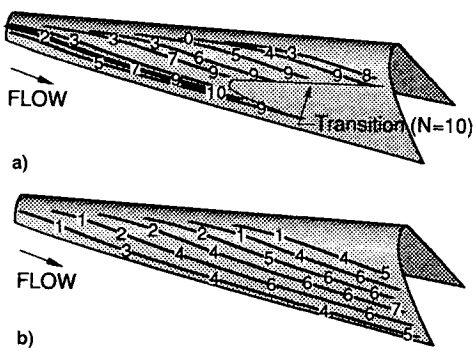

Fig. 5 N Factor calculations for case 1, α = 0 deg: a) f = 40 kHz and b) f = 0 KHz.

of the group velocity vector. For the traces shown, N = 0 at the initiation of the trace (the neutral point for three-dimensional disturbances at a given frequency). The traces were terminated when N reached a value of 10 (unless the aft portion of the body was reached first).

The results are presented for disturbance frequencies of 40 kHz (Fig. 5a) and 0 kHz (stationary disturbances) (Fig. 5b). The results for the 40-kHz disturbance indicate that the transition front is essentially parallel to the leading edge. The reduced level of crossflow near the symmetry plane results in N = 10 values being reached further downstream in this region. This explains the wedge-shaped transition front shown in Fig. 5a. When stationary disturbances are considered (Fig. 5b), N < 10 over the entire wing. The values of N ranged between 5–7 at the trailing section of the model. Thus, disturbances with the highest integrated growth rates are relatively high-frequency traveling disturbances. Of course, the final disturbance levels are dependent on the amplitude of the initial internalized disturbances, and, lacking this knowledge, the theory is unable to provide a definitive answer regarding the frequencies that will lead to transition. At any rate, due to much lower amplification rates, transition is unlikely to occur due to stationary crossflow disturbances (subject to the assumptions that the high frequency input disturbances exist and that the input amplitude levels are uniformly small across the frequency range).

The 40-kHz frequency specified above was approximately that frequency which first resulted in a value of N = 10. We found that the growth rates were not highly dependent on the value of the (higher) frequencies; i.e., by integrating growth rates for frequencies ranging from 30 to 40 kHz, the location where N reached 10 did not change significantly. This is demonstrated in Fig. 6 in which N = 10 locations are shown for 40-, 30-, and 20-kHz disturbances. The estimated transition fronts for the 30- and 40-kHz disturbance frequencies are nearly identical. The estimated front is further downstream for the 20-kHz case. The frequency response spectrum is thus relatively flat in this range.

Calculations for the wing at 4.5-deg incidence (case 4) are shown in Figs. 7a and 7b. Results shown in Fig. 7a represent 40-kHz disturbances, while those shown in Fig. 7b represent stationary disturbances. Figure 7a indicates that [compared to the case α = 0 deg (Fig. 5a)] the leading tip of the estimated location of the transition front has moved upstream, but the spanwise location of the front remains nearly unchanged. This behavior is somewhat surprising, considering the Re_{CF} distributions shown in Figs. 3a and 3b. Those figures indicated a significant increase in Re_{CF} levels near the leading edge as α is increased. Thus, one would have expected earlier transition, assuming that the process was crossflow-dominated. The integration distance was shorter, but the spanwise displacement from the leading edge, for values of N = 10, remained nearly unchanged at equivalent axial locations. For stationary disturbances (Fig. 7b), the value of N ranges from 6.5–7.5 at the end of the wing. These values are 10–20% higher than those for the α = 0-deg case.

We next investigate the effect of boundary-layer suction on the estimated location of the onset of transition. Two cases

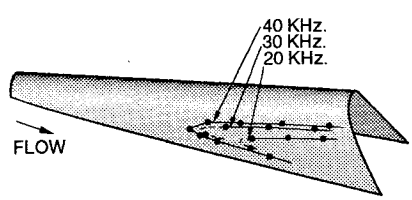

Fig. 6 Transition fronts for f = 40 and 30 kHz and f = 20 kHz for case 1.

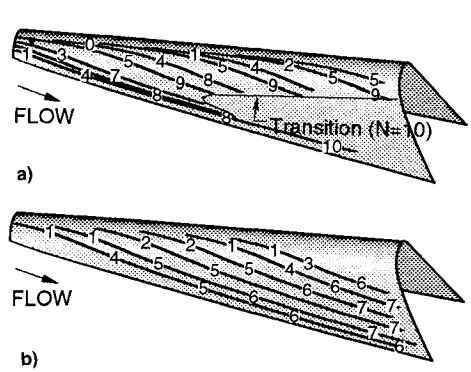

Fig. 7 N Factor calculations for case 4, α = 4.5 deg: a) f = 40 kHz and b) f = 0 kHz.

are presented (designated as cases 5 and 6). For case 5, the suction rate $q_s = (\rho_w v_w)/(\rho_\infty U_\infty)$ is specified as 0.0004 uniformly over the entire surface. For case 6, q_s is specified as a step function with $q_s = 0.0012$ at the leading edge, dropping to $q_s = 0.0001$ where the local spanwise distance from the leading edge is more than 10% of the local maximum span distance (see Fig. 8a). The suction rates in cases 5 and 6 are chosen such that the total mass flow rate in each case is approximately the same.

The effect of suction is to make the boundary layer thinner and also to reduce crossflow, which results in bringing the generalized inflection point closer to wall. Figures 8b and 8c show the spanwise variation of the crossflow Reynolds number and the displacement thickness with no suction (case 1) and with suction (cases 5 and 6). The Re_{CF} values are the lowest for the distributed (stepped) q_s case (the dip in this curve corresponds to step change in suction). Displacement thickness values are lower for case 6 near the attachment line compared to cases 1 and 5. However, case 6 displacement thickness values are larger than case 5 away from the attachment line region (beyond the step change in q_s). In Figs. 9a and 9b we present the N factor traces for the suction cases. For the uniform suction, N factor calculations (see Fig. 9a) show that the streamwise location of the initiation of transition is delayed considerably. The results for the stepped suction distribution, as shown in Fig. 9b, reveal N factors < 10 over the entire wing. Thus, suction is expected to be an effective means of delaying transition for these high-frequency (traveling) crossflow disturbances. Again, the N factors were not highly dependent on the value of the frequencies for 30 kHz $\leq f \leq$ 40 kHz.

We next investigate the effectiveness of wall cooling in stabilizing the boundary layer. Here, we have specified the wall temperatures as $T_w/T_\infty = 2$ and 2.6 (cases 7 and 8, respectively). For reference, the adiabatic wall temperature ratio for case 1 is $\approx$3.1. It is well-known that wall cooling has a considerable stabilizing effect for first mode instabilities. This is a consequence of the streamwise velocity profile inflection point being drawn closer to the wall. However, previous studies have revealed that wall cooling has only a weak stabilizing effect on crossflow instabilities at low supersonic speeds.[15] Figures 10a and 10b show the profiles of the normal derivatives $(\rho u')'$ and $(\rho v')'$ at a location close to the leading edge for the two cold wall cases, as well as the adiabatic wall case (case 1). The streamwise profiles (Fig. 10a) show lowering of the generalized inflection point $[(\rho u')' = 0]$ for case 8 and elimination of it for case 7 at this surface location. In

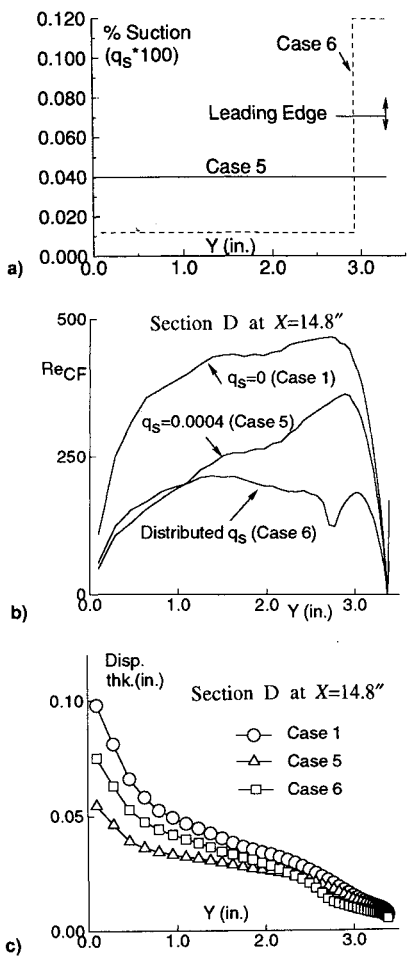

Fig. 8 Spanwise variation of a) input suction levels for cases 5 and 6, b) Re_{CF}, and c) displacement thickness, at $X = 14.8$ in.

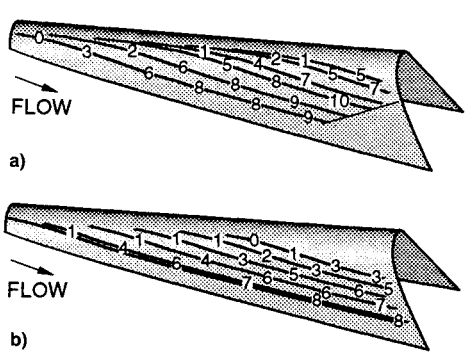

Fig. 9 N Factor calculations for a) case 5, $q_s = 0.0004$ and b) case 6, $q_s = 0.0012 \downarrow 0.0001$ (step function).

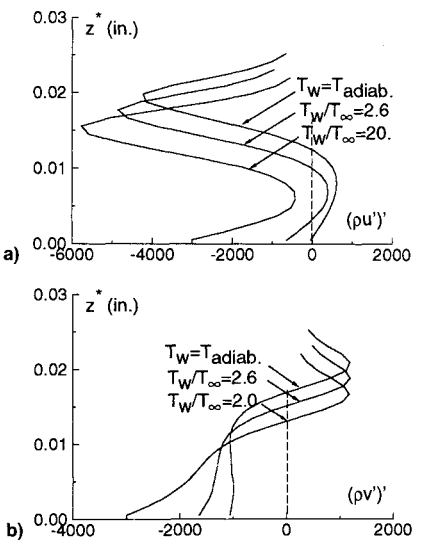

Fig. 10 Profiles of a) second derivative $(\rho u')'$ and b) second derivative $(\rho v')'$, at a point near the attachment line showing effect of cooling: cases 1, 7, and 8.

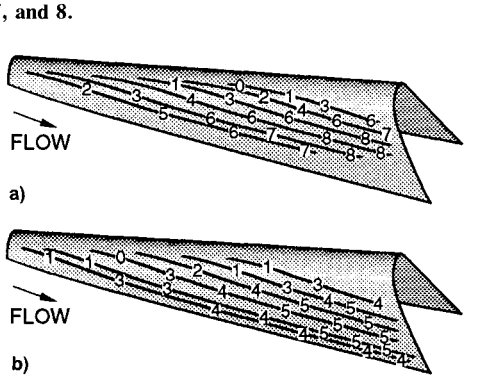

Fig. 11 N Factor calculations for case 7 with wall cooling: a) $f = 40$ kHz and b) $f = 0$ kHz.

the case of the crossflow profile, the inflection point cannot be totally eliminated by means of wall cooling; however, there is a mild stabilizing effect due to lowering of the inflection point. Figures 11a and 11b show the N factors for 40 kHz and stationary disturbances, respectively, for case 7 ($T_w/T_\infty = 2$). As was the case for the distributed suction, the wall cooling has diminished the growth rates to the extent that $N < 10$ over the entire body. From this, one may conclude that these high-frequency instabilities have a behavior similar to oblique TS disturbances as well.

Finally, we look at the effect of freestream Reynolds number on the transition location. Calculations reported here are for Re_∞ values of 1.2, 2.4, 4, and 6 million/ft (cases 9, 1, 10, and 11, respectively). From the mean flow perspective, the effect of lowering Re_∞ is to reduce Re_{CF} resulting from lower freestream velocities. In Figs. 12a and 12b we show this effect of Re_∞ variation on the displacement thickness and Re_{CF}. The increase in boundary-layer thickness due to lowering of the Re_∞ is more than offset by the decrease in U_∞, resulting in a net decrease in Re_{CF}. Note that changes in Re_∞ do not affect the C_p distribution or the percent crossflow appreciably. Figures 13a and 13b show N factor calculations for $Re_\infty = 1.2$ million/ft and $Re_\infty = 6$ million/ft, respectively. The N factor reaches values of 10 close to the leading edge for the higher

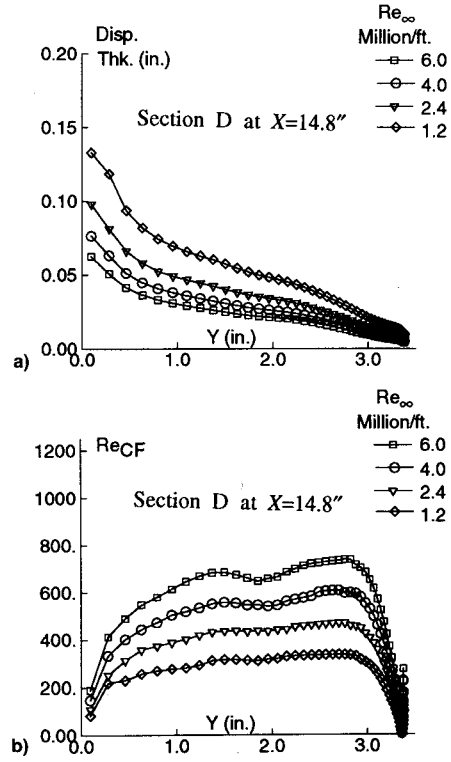

Fig. 12 Spanwise variation of a) displacement thickness and b) Re_{CF}, with Re_∞.

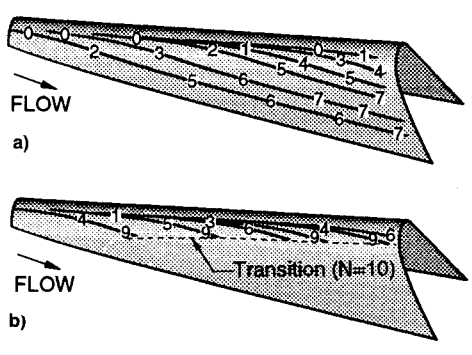

Fig. 13 N Factor calculations at $f = 40$ kHz for a) $Re_\infty = 1.2$ million/ft (case 9) and b) $Re_\infty = 6$ million/ft (case 11).

Re_∞ case, whereas N factor values are everywhere <7 for the $Re_\infty = 1.2$-million/ft case.

We now investigate the disturbance characteristics in greater detail. We do this by investigating the characteristics of the most unstable disturbances (at a given frequency) along six of the traces for the conditions of case 1. In Figs. 14a and 14b the evolution of the wave angle (measured with respect to the inviscid streamline) and the evolution of the wavelength are shown as a function of the axial distance. For stationary disturbances (Fig. 14a) the most amplified wave angle varies between 87–89 deg, depending on the axial location. These wave angles are characteristic of pure crossflow-type disturbances. The wavelength ($\lambda/\delta_{0.995}$) ranges from ≈4 at the neutral locations to ≈2 at the end of the wing. Again, these ratios are typical of crossflow disturbances. For the 40-kHz disturbances (Fig. 14b), the most amplified wave angles range from 70 to 80 deg, with the angle generally decreasing as the calculations proceed in the streamwise direction. Thus, the wave angles for these high-frequency disturbances are intermediate between those generally associated with pure crossflow instabilities and those associated with first mode instabilities. In addition, the wavelengths are in the range of ≈5.5 at the neutral point, decreasing to ≈4 at the end of the trace—somewhat higher than those associated with crossflow-dominated flows, but lower than those associated with first mode TS type disturbances.

The issues of mean flow accuracy and smoothness are of great importance in a stability calculation. The present approach of using the NS equations has the advantages that 1) viscous interaction effects are included, and 2) complicated

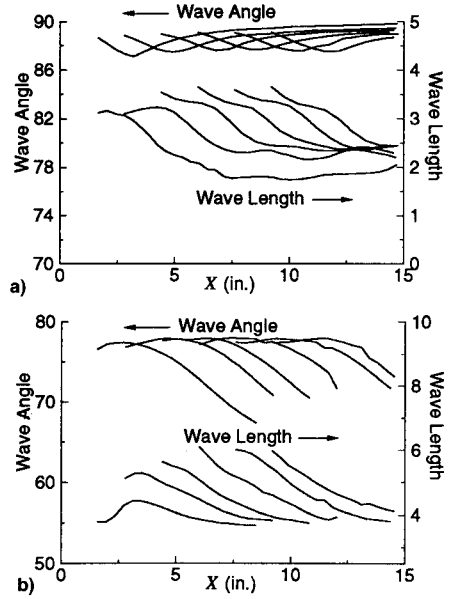

Fig. 14 Evolution of wave angle and wavelength of the most unstable disturbances: a) stationary and b) $f = 40$ kHz.

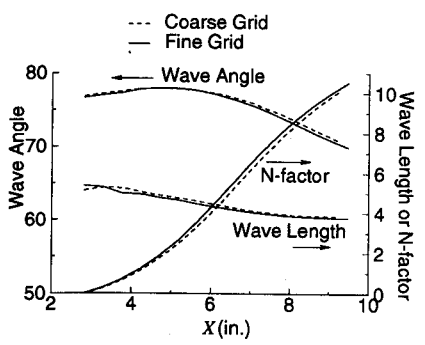

Fig. 15 Effect of normal grid resolution on stability parameters (case 1).

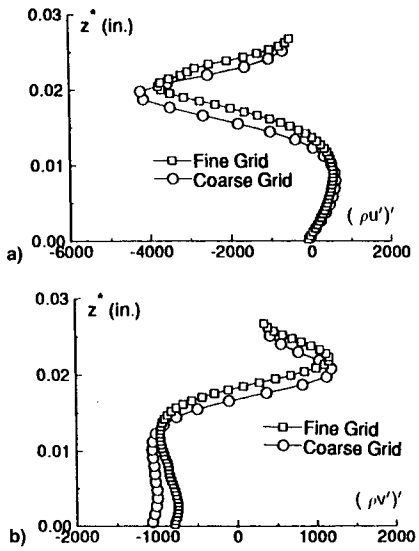

Fig. 16 Effect of normal grid resolution on the generalized inflection point: a) case 1, α = 0 deg and b) case 4, α = 4.5 deg.

(i.e., nonanalytic) aerodynamic flows can be calculated. The accuracy of solution is a function of the grid, the algorithm, and convergence to steady state. The important issue for laminar boundary layers is obtaining grid-converged results.[16] Reference 9 compares the upwind-differenced code CFL3D with a central-differenced code and concludes that 1) CFL3D is the more accurate code for a given grid, and 2) depending on the case, 49–65 points in the normal direction are adequate for grid convergence as far as pressure and force coefficients are concerned. As indicated in Ref. 16, larger normal grid resolution may be required for laminar boundary-layer profiles.

To resolve the grid resolution issue, and also to verify adequate smoothness of the input boundary-layer profiles, the case 1 calculation was repeated with 121 points in the surface-normal direction (the 97 × 53 grid in the body surface directions was considered adequate, and therefore remained unchanged). This calculation produced mean flow profiles which had on the average 60 points in the boundary layer, compared to 30 points for the previous results. In Fig. 15, we present the wave angle, wavelength, and N factor values corresponding to a single trace for the coarse and fine grid runs. The results indicate that there is little variation in these stability parameters.

In Fig. 16 we present the second derivative profiles $(\rho u')'$ and $(\rho v')'$ at a location close to the leading edge (similar to Fig. 10), for the coarse and fine grid mean flow computation. The profiles corresponding to the fine grid have their inflection points shifted slightly outward at this location. However, an examination of profiles at other locations revealed that this difference is much smaller at other locations.

An optimum grid for a swept wing calculation such as this, should then have about 30–50 points in the boundary layer, representing an optimum tradeoff between accuracy and computational cost. The results presented here correspond to the lower end of this range. It may be noted that a finer grid does not necessarily imply a smoother profile, especially close to the wall. This is in contrast with classical boundary-layer solutions, where profile smoothness increases directly in proportion to increased normal grid resolution.

Summary

Linear stability calculations were made to estimate the location of the onset of transition on a highly swept supersonic wing leading edge which is to be tested in the NASA Langley M = 3.5 SSLDP tunnel. The present study is essential in determining the test conditions and measurement requirements for the experimental study. A parametric study was performed to assess the effects of freestream conditions (angle of attack, Reynolds number) and flow control techniques (suction and wall cooling). Navier-Stokes mean flow profiles were used for the three-dimensional linear stability analysis, and a grid refinement study revealed that 30–50 points in the boundary layer provided adequate accuracy. The stabilizing effect of suction and wall cooling were verified. The angle-of-attack variation in the range studied did not produce any appreciable change in the predicted transition front.

Linear stability analysis of a fully three-dimensional and nonanalytic supersonic geometry using solution profiles from the Navier-Stokes equations has been accomplished. This study shows that for accurate supersonic laminar wing design, the present approach of using Navier-Stokes solution is feasible on reasonably sized grids. The present procedure does not have the limitations on mean flow accuracy imposed by three-dimensional boundary-layer methods.

Acknowledgments

V. Iyer would like to acknowledge support received under NASA Langley Research Center Contract NAS1-18585 from the Theoretical Flow Physics Branch of the Fluid Mechanics Division. R. E. Spall acknowledges support received from the University of South Alabama Research Committee.

References

[1]Harris, R. V., and Hefner, J. N., "NASA Laminar Flow Program—Past, Present and Future," *Proceedings of a Symposium on Research in National Laminar Flow and Laminar-Flow Control*, NASA CP-2487, Pt. 1, March 1987, pp. 1–25.

[2]Bushnell, D. M., Malik, M. R., and Harvey, W., "Transition Prediction in External Flows with Linear Stability Theory," International Union of Theoretical and Applied Mechanics Symposium Transsonicum III, Gottingen, Germany, May 1988.

[3]Malik, M., "Stability Theory for Laminar Flow Control Design," Vol. 123, Progress in Astronautics and Aeronautics, AIAA, Washington, DC, 1990.

[4]Spall, R. E., and Malik, M., "Linear Stability of Three-Dimensional Boundary-Layers over Axisymmetric Bodies at Incidence," *AIAA Journal*, Vol. 30, No. 4, 1992, pp. 905–913.

[5]Spall, R. E., and Wie, Y.-S., "Stability Theory and Transition Prediction Applied to a General Aviation Fuselage," *Journal of Aircraft*, Vol. 30, No. 2, 1993, pp. 161–167.

[6]Cebeci, T., Chen, H. H., Arnal, D., and Huang, T. T., "Three-Dimensional Linear Stability Approach to Transition on Wings and Bodies of Revolution at Incidence," *AIAA Journal*, Vol. 29, No. 12, 1991, pp. 2077–2085.

[7]Malik, M., "COSAL—a Black Box Compressible Stability Code for Transition Prediction in Three-Dimensional Boundary-Layers," NASA CR-165925, May 1982.

[8]Thomas, J., Taylor, S., and Anderson, W., "Navier-Stokes Computation of Vortical Flows over Low Aspect Ratio Wings," AIAA Paper 87-0207, Jan. 1987.

[9]Bonhaus, D. L., and Wornom, S. F., "Comparison of Two Navier-Stokes Codes for Attached Transonic Wing Flows," *Journal of Aircraft*, Vol. 29, No. 1, 1992, pp. 101–107.

[10]Iyer, V., "Assessment of Meanflow Solutions for Instability Analysis of Transitioning Flows," AIAA Paper 91-1638, June 1991.

[11]Malik, M., and Orzag, S., "Efficient Computation of the Stability of Three-Dimensional Boundary-Layers," AIAA Paper 81-1277, June 1981.

[12]Gaster, M., "A Note on the Relation Between Temporally Increasing and Spatially Increasing Disturbances in Hydrodynamic Instability," *Journal of Fluid Mechanics*, Vol. 14, Pt. 2, Oct. 1962, pp. 222–224.

[13]Poll, D. I. A., "Transition Prediction in Three-Dimensional Flows," Special Course on Stability and Transition of Laminar Flow, AGARD Rept. 709, March 1984.

[14]Malik, M. R., Balakumar, P., and Chang, C. L., "Linear Stability of Hypersonic Boundary Layers," NASP Paper 189, April 1991.

[15]Lekoudis, S. G., "Stability of the Boundary Layer on a Swept Wing with Wall Cooling," *AIAA Journal*, Vol. 18, No. 9, 1980, pp. 1029–1035.

[16]Jou, W.-H., Wigton, L. B., Allmaras, S. R., Spalart, P. R., and Yu, N. J., "Towards Industrial-Strength Navier-Stokes Codes," Fifth Symposium on Numerical and Physical Aspects of Aerodynamic Flows, California State Univ., Long Beach, CA, Jan. 1992.